Iron and carbon isotope evidence for ecosystem and environmental diversity in the ~2.7 to 2.5 Ga Hamersley Province, Western Australia

Andrew D. Czaja [a,b,*], Clark M. Johnson [a,b], Brian L. Beard [a,b], Jennifer L. Eigenbrode [c], Katherine H. Freeman [d], Kosei E. Yamaguchi [b,e,f]

[a] Department of Geoscience, 1215 W. Dayton Street, University of Wisconsin, Madison, WI 53706, USA
[b] NASA Astrobiology Institute, University of Wisconsin, Madison, WI 53706, USA
[c] NASA Goddard Space Flight Center, Code 699.0, Greenbelt, MD 20771, USA
[d] Department of Geosciences, The Pennsylvania State University, University Park, PA 16802, USA
[e] Department of Chemistry, Toho University, 2-2-1 Miyama, Funabashi, Chiba 274-8510, Japan
[f] Precambrian Ecosystem Laboratory, Japan Agency for Marine-Earth Science and Technology, 2-15 Natsushima, Yokosuka, 237-0061, Japan

ARTICLE INFO

ABSTRACT

The largest excursion in kerogen $\delta^{13}C$ and bulk/mineral $\delta^{56}Fe$ values yet measured in the ancient rock record occurs in rocks of ~2.7 to 2.5 Ga age. New Fe isotope data integrated with previously collected C isotope data on the same samples document the metabolic diversity of microbial communities in the Neoarchean Hamersley Province of the Pilbara Craton in Western Australia. Samples of shales, carbonates, and mixed carbonate/shale lithologies were collected from three drill cores; two cores from the depocenter of the province and one from the margin. Shallow-water clastic/carbonate rocks deposited in the center of the province (Tumbiana Formation) record kerogen $\delta^{13}C$ values that indicate C cycling by various anaerobic or aerobic methane pathways, but the restricted range in $\delta^{56}Fe$ values indicates little or no Fe redox cycling. Deep-water sediments deposited contemporaneously in both parts of the Hamersley Province (Jeerinah Formation) record slightly positive $\delta^{56}Fe$ values in the relatively shallower and suboxic margin, but strongly negative $\delta^{56}Fe$ values in the deeper euxinic depocenter of the province, a pattern consistent with Fe cycling via a basin Fe shuttle, driven by bacterial dissimilatory iron reduction (DIR). Kerogen $\delta^{13}C$ values from these units indicate coupling of microbial Fe cycling to aerobic methanotrophy or anaerobic oxidation of methane. Younger black shales, intercalated with iron formation (Marra Mamba Iron Formation) in the depocenter, record a shift to near-zero $\delta^{56}Fe$ values reflecting an Fe budget dominated by hydrothermal and clastic sources. However, time-equivalent, Fe-rich carbonate/shale lithologies deposited on the margin of the province (Carawine Dolomite) have $\delta^{56}Fe$ values that steadily decrease from near zero to strongly negative values. These relatively Fe-rich carbonates may reflect a carbonate trap of a DIR-driven Fe shuttle, similar to the sulfidic trap in the euxinic portion of the Jeerinah Formation. In contrast, younger shallow-water carbonates deposited by turbidity currents in relatively deep water in the center of the province (Wittenoom Formation), have $\delta^{56}Fe$ values that correlate with Fe concentrations, a pattern that indicates Fe cycling by Rayleigh fractionation through precipitation of iron oxides from aqueous ferrous iron.

© 2010 Elsevier B.V. All rights reserved.

1. Introduction

The interplay between the biosphere, lithosphere, hydrosphere, and atmosphere has produced a complex evolution of microbial metabolisms that significantly affect the geochemical and mineralogical compositions of surface environments. The relative evolution of various microbial metabolisms may be constrained through phylogenetic reconstructions (e.g., Woese and Fox, 1977; Canfield and Raiswell, 1999; Battistuzzi et al., 2004; Zerkle et al., 2005), and a sense of time may

be gained from the rate of evolution of molecules that are widely distributed and highly conserved (e.g., Ochman and Wilson, 1987; Canfield and Teske, 1995; Sheridan et al., 2003). Ultimately, however, quantitative constraints on temporal changes in microbial metabolisms on the ancient Earth depend upon geologic and geochemical data obtained from well-dated and well-preserved sedimentary rocks whose global and/or local context is understood.

In addition to microfossils and molecular fossils (biomarkers), the presence and temporal distribution of metabolisms can be traced using the abundances and isotopic compositions of metabolically cycled elements in sedimentary rocks, such as carbon, sulfur, and iron (e.g., Yamaguchi et al., 2004). Measurement of the isotopic compositions of C and S has proven valuable for tracing the evolution of metabolisms on the early Earth, including photosynthesis, methanotrophy, and

methanogenesis (e.g., Eigenbrode and Freeman, 2006), as well as sulfate- and elemental-sulfur reduction, sulfide oxidation, and sulfur disproportionation (e.g., Canfield, 2001). The largest excursions in kerogen C isotope compositions and mass-independent S isotope fractionations in sulfides occur between ~2.7 and 2.4 Ga (e.g., Farquhar and Wing, 2003; Eigenbrode and Freeman, 2006), suggesting major changes in the C and S cycles. Of the redox-sensitive metals cycled by microbes, Fe has been the focus of numerous biological studies (e.g., Widdel et al., 1993; Lovley, 2004), and the isotopic record of microbial Fe cycling is now beginning to be understood (Johnson et al., 2008b).

Redox Fe cycling seems the most likely explanation for producing the large Fe isotope variations measured in Precambrian marine sedimentary rocks, given the large isotopic fractionations that occur between Fe^{3+} and Fe^{2+} species (e.g., Polyakov and Mineev, 2000; Schauble et al., 2001; Welch et al., 2003; Anbar et al., 2005). Although Fe isotope fractionations can be produced by changes in chloride speciation (Hill et al., 2009), at seawater salinities these effects are not significant relative to the fractionations between ferric and ferrous Fe species. There is consensus that the zero to positive $\delta^{56}Fe$ values for rocks of >3.1 Ga age reflect partial oxidation of marine hydrothermal Fe^{2+}_{aq}, suggesting that the oxidant was limited (e.g., Dauphas et al., 2004; Johnson and Beard, 2006; Whitehouse and Fedo, 2007). More controversial are large decreases in $\delta^{56}Fe$ values of 3.1 to 2.5 Ga marine sedimentary rocks, which are coincident with large changes in C and S isotope ratios (Johnson et al., 2008b). Focusing only on Fe isotope data from rocks younger than 2.7 Ga, Rouxel et al. (2005) and Anbar and Rouxel (2007) proposed that oxidation of marine hydrothermal Fe^{2+}_{aq} during banded iron formation (BIF) genesis, or oxide precipitation on continental shelves, produced negative $\delta^{56}Fe$ values in seawater via Rayleigh distillation followed by incorporation into sulfide-rich marine sedimentary rocks. In contrast, Johnson et al. (2008a,b) argue that extensive oxide precipitation will result in only small quantities of isotopically fractionated Fe and therefore an alternative such as bacterial dissimilatory iron reduction (DIR) is required to produce negative $\delta^{56}Fe$ values for Fe-rich rocks such as BIFs or Fe-rich shales.

Here we report new Fe isotope and geochemical data on the same samples for which organic- and carbonate-C isotope compositions were previously measured, collected from the Hamersley Province of Western Australia (Fig. 1) and spanning the interval of large C and Fe isotope changes in Neoarchean (2.72 to 2.57 Ga) marine sedimentary rocks. Samples were collected from two parts of the province that record different paleoenvironments, allowing us to determine the relative importance of abiological Fe pathways versus microbial Fe metabolisms. Detailed and comprehensive study of multiple isotopes and whole-rock geochemical analyses allows for a complete view of the distribution of mineral phases, and a fuller understanding of the cycling of metabolically relevant elements such as C, S, and Fe.

2. Materials and methods

We analyzed fifty-eight samples of shales, carbonates, and mixed shale/carbonate lithologies from three diamond drill cores. Two of the cores (WRL1 and SV1) were recovered from the "main outcrop area" in the center of the province near Wittenoom, and one core (RHDH2a) from the east-northeastern "Oakover River area" in the Ripon Hills region (Fig. 1).

2.1. Geologic setting

The core samples studied here were collected from the 2.77 to 2.43 Ga Mount Bruce Megasequence Set of the Pilbara Craton in northwestern Western Australia (Fig. 1), a unit composed of volcanic and sedimentary sequences deposited on an Archean granite–greenstone terrane. The depositional history in the main outcrop area has been described in detail by Trendall and Blockley (1970),
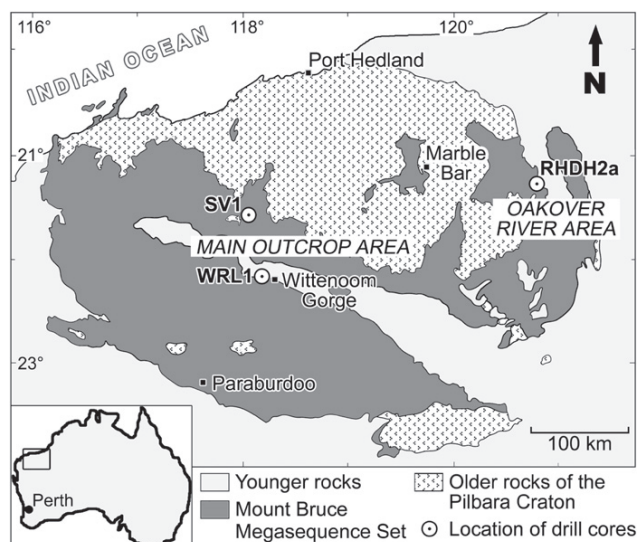

Fig. 1. Geologic map of the Pilbara Craton of northwestern Western Australia (adapted from Thorne and Trendall, 2001). Shown are locations of drill cores sampled; WRL1 and SV1 from the main outcrop area, near the depocenter of the Hamersley Province, and RHDH2a in the Oakover River area, in the Ripon Hills, near the margin.

Blake and Barley (1992), Blake (1993), Blockley et al. (1993), Lascelles (2000), and Thorne and Trendall (2001), and that of the Oakover River area by Williams (1989), Simonson et al. (1993), and Hassler et al. (2005). The sedimentology of the WRL1, SV1, and RHDH2a cores was reported by Meakins (1987), Lawrence (1985), and Richards (1985), respectively. The stratigraphy of these regions of the Hamersley Province is summarized in Fig. 2. The cores studied experienced only relatively low-grade metamorphism, in the prehnite–pumpellyite–epidote zone described by Smith et al. (1982). The drill cores were sampled from portions showing minimal pyrite oxidation and the outer surfaces were removed. There is no evidence in the samples studied for large-scale redistribution of Fe, such as from secondary pyritization, or for post-depositional fluid flow through the rocks, as indicated by $\delta^{18}O$ values for carbonate in the samples that fall within the range of unaltered Neoarchean carbonates (J. Eigenbrode, unpub. data). Details of the depositional environments of each region are reported in the online Supplementary material.

Layers of impact ejecta deposited in each region of the province provide key correlations. Hassler et al. (2005) and Rasmussen et al. (2005) interpreted impact layers in the Jeerinah and Carawine units (Fig. 2) to reflect the same event, consistent with ages of 2629 ± 5 Ma (Trendall et al., 2004) and 2630 ± 6 Ma (Rasmussen et al., 2005), respectively. In the main outcrop area, this layer is situated ~2.5 m below the Jeerinah/Marra Mamba contact (Hassler et al., 2005), but in the Oakover River area, it is ~60 m above the Jeerinah/Carawine contact (Rasmussen et al., 2005). Thus, the Carawine Dolomite in the east-northeast part of the province was deposited at the same time as the Marra Mamba Iron Formation (IF) in the center, and is not age-equivalent to the dolomite-dominated Wittenoom Formation (Hassler et al., 2005; Rasmussen et al., 2005). Here we use a chronostratigraphic model (Fig. 2) to temporally correlate our samples from the two regions, based on these impact spherule layers, geochronological data (Blake et al., 2004; Trendall et al., 2004; Rasmussen et al., 2005, and references therein), and integrated depositional rates (Trendall et al., 2004); details are described in the online Supplementary material.

2.2. Materials

The samples studied here are splits from cores collected by Eigenbrode and Freeman (2006). Care was taken to sample, on a fine
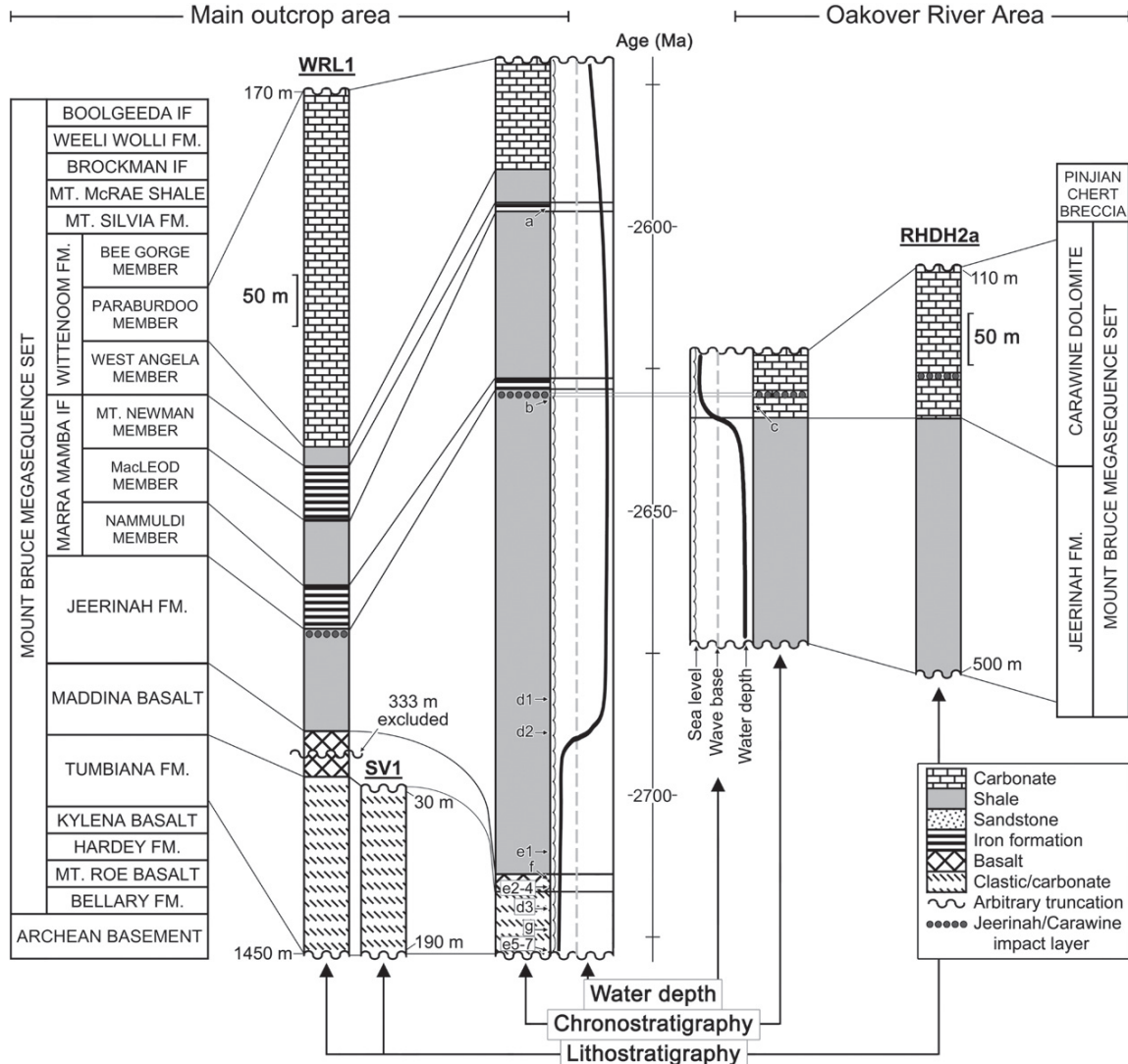
Fig. 2. Lithostratigraphic and chronostratigraphic relationships of the studied drill cores. The left side of the figure shows the stratigraphy of the WRL1 and SV1 cores from the main outcrop area based on regional lithostratigraphy described by Trendall et al. (2004) and core logs (Lawrence, 1985; Meakins, 1987). The right side illustrates the stratigraphy of the RHDH2a core from the Oakover River area based on core logs (Richards, 1985). The scale on each core shows the depth ranges sampled. The age of each sample, and thus the duration of each geological unit, was determined using a chronostratigraphic model based on geochronological data, impact spherule layers, and integrated depositional rates (see Supplementary material for a detailed description). The horizontal tie line connecting the chronostratigraphic columns indicates the simultaneous deposition of the Jeerinah and Carawine impact spherule layers in each region of the province. Letters in the center of the figure signify U–Pb ages from the literature: $a = 2597 \pm 5$ Ma (Trendall et al., 1998); $b = 2629 \pm 5$ Ma (Trendall et al., 2004); $c = 2630 \pm 6$ Ma (Rasmussen et al., 2005); $d1 = 2684 \pm 6$ Ma, $d2 = 2690 \pm 16$ Ma, $d3 = 2715 \pm 6$ Ma (Arndt et al., 1991); $e1 = <2715 \pm 2$ Ma, $e2 = 2715 \pm 2$ Ma, $e3 = 2713 \pm 3$ Ma, $e4 = 2718 \pm 3$ Ma, $e5 = 2721 \pm 4$ Ma, $e6 = <2727 \pm 5$ Ma, $e7 = 2724 \pm 5$ Ma (Blake et al., 2004); $f = 2717 \pm 2$ Ma (Wingate, 1999), and $g = 2719 \pm 6$ Ma (Nelson, 2001). Schematic water depth curves for each region of the province are shown next to the chronostratigraphic columns, with sea level and wave base indicated. The curves are qualitative and meant to show relative differences between the various depositional environments. The curves are based on literature descriptions (see Supplementary material online).

scale, the exact depth intervals as these authors to allow direct comparison of data from their study with new data obtained here. Some of the depth intervals used by Eigenbrode and Freeman (2006) were subdivided based on lithologic differences (see Tables S1 and S2). Data collected from these samples were integrated with data from 31 samples studied by Yamaguchi et al. (2005) that were collected from the same cores.

2.3. Sample preparation

Samples were prepared for chemical and isotopic analyses following methods described by Yamaguchi (2002) and Yamaguchi et al. (2005). Powdered samples were split for whole-rock geochemistry and iron isotope analyses. Whole-rock major oxide, carbonate,

total sulfur, total organic carbon, and ferrous iron analyses were performed by Activation Laboratories of Ancaster, ON Canada. Hydrochloric acid-extractable Fe and carbonate analyses, as well as XRD powder analyses, were performed at the University of Wisconsin–Madison. Full sample preparation and analytical details are reported in the online Supplementary material.

2.4. Analytical procedures for Fe isotope analysis

Following digestion of the samples and purification of the iron by ion exchange chromatography, Fe isotope compositions were measured by multi-collector, inductively-coupled plasma mass spectrometry (MC-ICP-MS; Micromass, *IsoProbe*) at the University of Wisconsin–Madison. Detailed analytical procedures are reported by

Beard et al. (2003), Albarède and Beard (2004), and in the online Supplementary material. Iron isotope data are reported in standard delta notation as δ^{56}Fe values in units of per mil (‰) relative to the average of igneous rocks:

$$\delta^{56}Fe = \left(\left({}^{56}Fe/{}^{54}Fe\right)_{Sample} \Big/ \left({}^{56}Fe/{}^{54}Fe\right)_{Ig\ Rxs} - 1 \right) \times 10^3. \qquad (1)$$

The IRMM-014 standard has a δ^{56}Fe value of -0.09‰ on this scale (Beard et al., 2003).

3. Results

All isotopic and geochemical data collected are reported online in Tables S1 and S2. A broad range of Fe isotope compositions were measured, varying between δ^{56}Fe $= +0.38$ and -2.43‰ for all samples, including those of Yamaguchi et al. (2005) (Table S2). Kerogen C isotope compositions measured on the same samples range from $\delta^{13}C_{ker} = -27.7$‰ to -49.7‰ (Table S2), whereas $\delta^{13}C_{carb}$ values for carbonate-rich units are near zero [data from Eigenbrode and Freeman (2006)]. The dominant Fe-bearing minerals in each sample were determined based on whole-rock major element, reactive Fe, bulk S, total organic carbon, and CO_2 data, as well as XRD spectra (see Supplementary material). In addition, we classified samples based on lithology, grouping samples as carbonate, carbonate-rich shale, shale, and silicified carbonate, based on CO_3–Al_2O_3–SiO_2 relations (Fig. 3), as well as other data.

The measured Fe isotope compositions (Tables S1 and S2) reflect the effects of Fe sources, lithology, mineralogy, and depositional environment. The δ^{56}Fe values of the very shallow-water Tumbiana Formation are close to the crustal average (δ^{56}Fe ≈ 0‰, Fig. 4A). With increasing paleo water depth (Fig. 2), the Jeerinah Formation shales of the main outcrop area, which have an Fe mineralogy dominated by pyrite and oxides, have δ^{56}Fe values that decrease from -0.42 to -1.54‰, with a slight increase near the top to δ^{56}Fe $= -1.20$‰. In the Marra Mamba IF, which has variable lithology (shale, carbonate-rich shale, and carbonate) and Fe mineralogy (including Fe-carbonate, phyllosilicates, siderite, and magnetite), δ^{56}Fe values are highly variable in the lower and upper portions, at transitions to other units, and close to δ^{56}Fe $= 0$‰ in the middle (Fig. 4A). The Fe isotope compositions of shales and carbonates of the West Angela member, the lowermost unit of the Wittenoom Formation (Fig. 2), are also variable (δ^{56}Fe $= -0.87$ to $+0.13$‰). Most samples of the dominantly carbonate deposits of the overlying Paraburdoo member have variably low δ^{56}Fe values (-0.23 to -1.68‰). In the Oakover River area, the shales of the lower Jeerinah

Formation, in which phyllosilicates comprise the dominant Fe minerals, δ^{56}Fe values range from -0.06 to $+0.38$‰, and all but two of the measured values are positive. Notably, the upper Jeerinah Formation and Carawine Dolomite record a major excursion in Fe isotope composition (δ^{56}Fe $= -2.43$ to $+0.36$‰; Fig. 4A).

Shales studied here have a wide range of Fe isotope compositions and Fe contents (Fig. 4A and B, and Fig. S5). Samples from the Tumbiana and Jeerinah formations show no clear relation between δ^{56}Fe values and total Fe content (Fe$_T$) (Fig. 4A and B, and Fig. S5A and B). The Jeerinah Formation shales from each part of the province have similar Fe$_T$ contents, but different average δ^{56}Fe values (Fig. 4A and B). The Marra Mamba IF samples generally have high Fe$_T$ contents, and a wide range in δ^{56}Fe values (Fig. 4A and B), but samples that have low Fe$_T$ contents also have low δ^{56}Fe values (Fig. S5C); these samples occur in the transition immediately above the Jeerinah Formation. In contrast, samples from the Carawine Dolomite, which is age-correlative with the Marra Mamba IF, have much lower Fe$_T$ contents, although these values are significantly higher than the average Archean shelf carbonate Fe$_T$ content (Fig. 4B). In the Carawine samples that have the lowest δ^{56}Fe values (those of the upper part of the unit; Table S1 and Fig. 4A), a negative correlation between δ^{56}Fe values and Fe$_T$ contents is suggested (Fig. 5C). Samples from the Wittenoom Formation that have an Fe mineralogy dominated by Fe-carbonate have δ^{56}Fe values that correlate with Fe$_T$ (Fig. 4A and B, and Fig. S5D), and the samples that have the lowest Fe contents fall below that of the average Archean shelf carbonate value. Samples from the Wittenoom Formation that have a phyllosilicate-dominated Fe budget have a generally negative correlation between δ^{56}Fe values and Fe$_T$ (Fig. S5D).

Kerogen C isotope compositions for the samples vary greatly, encompassing $\delta^{13}C_{ker}$ values characteristic of photosynthetic carbon fixation and more negative values that require methane cycling (Eigenbrode and Freeman, 2006; Fig. 4C). Most units do not show a significant correlation between δ^{56}Fe and $\delta^{13}C_{ker}$ values (Fig. 4A, C, and Fig. S5E–H), but an important exception is the Carawine Dolomite, in which there is a slight positive correlation between δ^{56}Fe and $\delta^{13}C_{ker}$ values (Fig. S5G). As is described in Section 4.2.3, this relation correlates with environmental facies.

The relative degree of Fe enrichment for shales is determined using total Fe to Al ratios (Fe$_T$/Al$_T$), following Lyons and Severmann (2006). For the Jeerinah Formation, δ^{56}Fe values are, on average, somewhat negatively correlated with Fe$_T$/Al$_T$ ratios; importantly, shales of the Jeerinah Formation of the main outcrop area are relatively more iron-rich and have significantly lower δ^{56}Fe values than those of the Oakover River area (Fig. 5A). Relative to Fe$_T$/Al$_T$–δ^{56}Fe relations
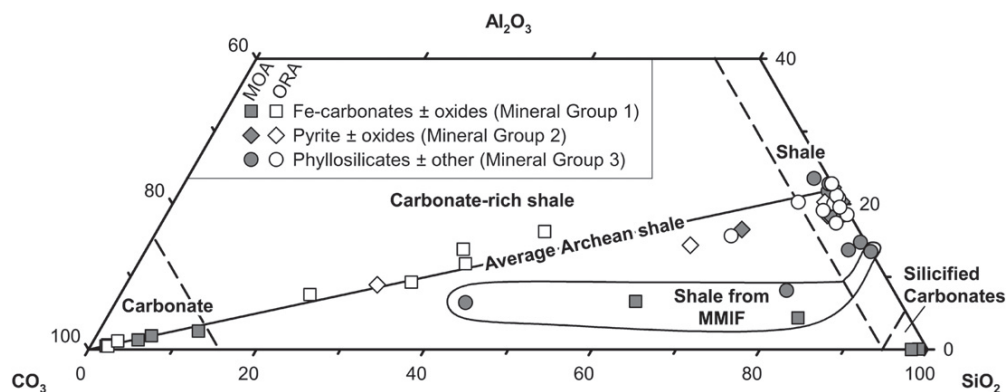
Fig. 3. The distribution of rock types sampled from the main outcrop area (MOA, gray symbols) and the Oakover River area (ORA, open symbols). The samples analyzed are divided into three main lithologies, carbonates, carbonate-rich shales, and shales, which are separated by dashed diagonal lines. Symbols used are based on mineral groups from Table S2 in the Supplementary material. The solid diagonal line represents the mixing line for average Archean shales (Taylor and McLennan, 1985). The symbols that plot significantly below the mixing line represent shale samples from the Marra Mamba Iron Formation (outlined) and two silicified carbonates (near the SiO$_2$ vertex). Note that only 46 of 89 samples [including those of Yamaguchi et al. (2005)] are plotted here. The remaining samples were of insufficient size for major oxide analysis.
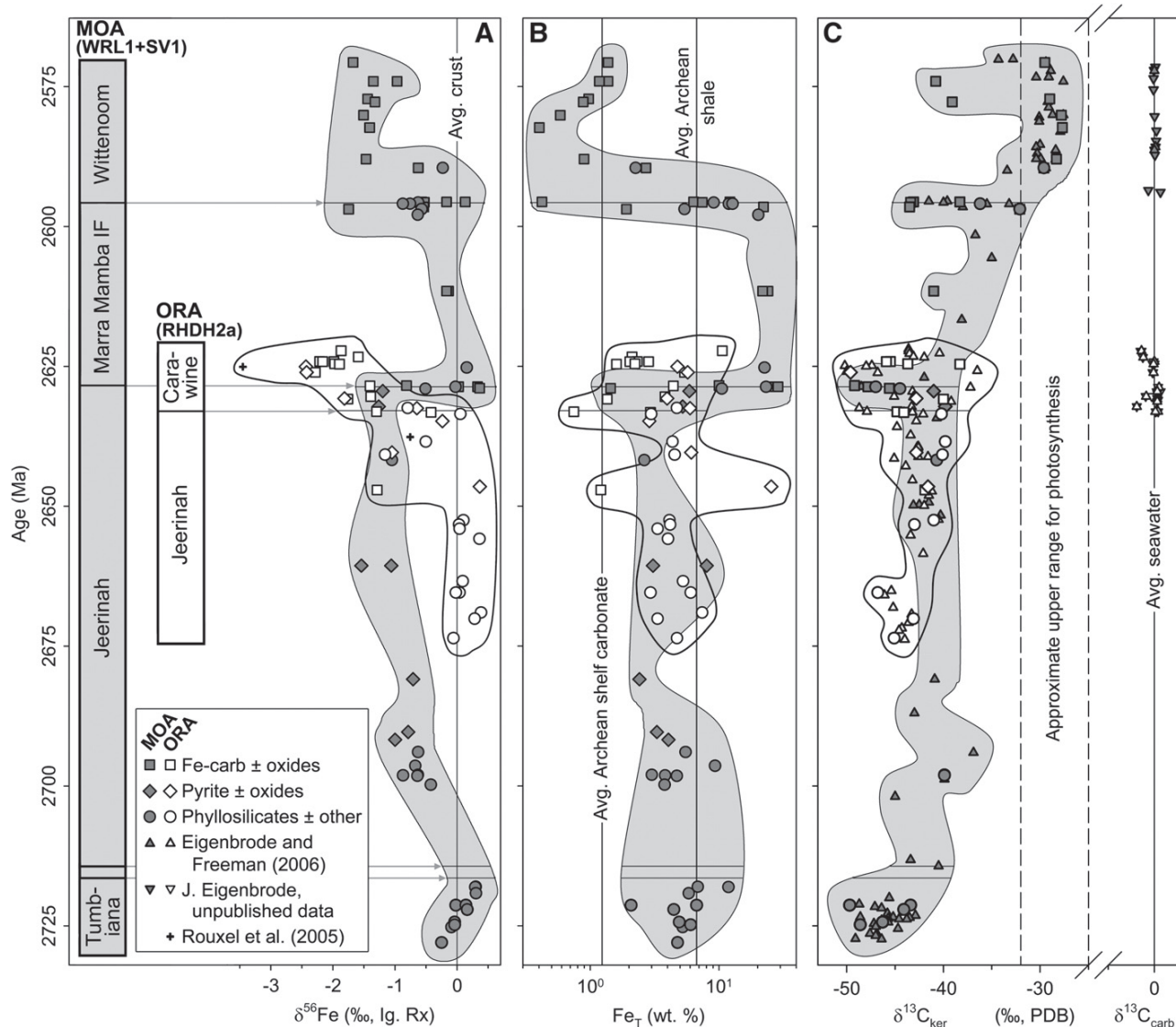
Fig. 4. Time profiles of isotopic and total Fe data for two regions of the Hamersley Province (see Table S2 in online Supplementary material). Shown are values for δ^{56}Fe in units of per mil (‰) relative to the average of igneous rocks (A), total Fe (Fe$_T$) in wt.% (B), and carbon isotope data in units of per mil relative to the Pee Dee Belemnite standard (C) for kerogens ($\delta^{13}C_{ker}$; Eigenbrode and Freeman, 2006), and for carbonates ($\delta^{13}C_{carb}$; Eigenbrode and Freeman, 2006, and J. Eigenbrode, unpublished data). In part A, the data include two δ^{56}Fe analyses of pyrites measured by Rouxel et al. (2005) from core RHDH2a. The vertical reference line in part A represents the δ^{56}Fe value of average crustal rocks (δ^{56}Fe = 0‰). The vertical lines in part B indicate the average Fe$_T$ values of Archean shelf carbonates (Fe$_T$ = 1.24 wt.%; Veizer et al., 1990) and Archean shales (Fe$_T$ = 6.72 wt.%; Taylor and McLennan, 1985). In part C the rightmost reference line represents the average seawater δ^{13}C value and the dashed vertical lines represent an approximate range of expected $\delta^{13}C_{ker}$ values for biomass produced via photosynthesis (Eigenbrode and Freeman, 2006, and references therein). The symbols are the same as those in Fig. 3. All $\delta^{13}C_{ker}$ data were measured by Eigenbrode and Freeman (2006), but the samples that were also analyzed in this study are plotted in part C using symbols based on Fe mineralogy. For reference, the horizontal lines in parts A, B, and C mark the boundaries between each geologic formation shown in the chronostratigraphic columns on the left side of part A (cf. Fig. 2).

determined for clastic sediments from the Black Sea (Severmann et al., 2008; Fig. 5), the data from the Jeerinah Formation extend to higher Fe$_T$/Al$_T$ ratios and lower δ^{56}Fe values. Fe$_T$/Al$_T$ and δ^{56}Fe values of the carbonate-rich shales of the Carawine Dolomite also are negatively correlated (Fig. 5B). It is important to note that these relations are not an artifact of different carbonate contents, because the range of carbonate contents for the samples studied by Severmann et al. (2008) is the same as the data plotted in Fig. 5 from this study.

For carbonate-rich samples, including those of the Wittenoom Formation and Carawine Dolomite, we also compare relative Fe enrichments or depletion using the ratio of HCl-extractable Fe to carbonate content (Fe$_{T-HCl}$/C$_{carb}$) (Fig. 6), which provides an assessment of the Fe contents of the carbonates. The Wittenoom Formation samples generally show a good correlation of decreasing δ^{56}Fe values

with decreasing Fe contents in carbonate, whereas the Carawine Dolomite samples do not have such a correlation; indeed, some samples with relatively high Fe contents have very negative δ^{56}Fe values (Fig. 6).

4. Discussion

Neoarchean ecosystems consisted of photoautotrophs (anoxygenic and oxygenic photosynthetic bacteria) and chemoautotrophs (e.g., methanogens and acetogens), as well as anaerobic heterotrophs (fermentors, Fe-reducing bacteria, sulfate-reducing bacteria, and anaerobic methylotrophs) and aerobic heterotrophs (e.g., Brocks et al., 1999; Xiong et al., 2000; Schidlowski, 2001; van Zuilen et al., 2002; Yamaguchi, 2002; Rosing and Frei, 2004; Kopp et al., 2005;
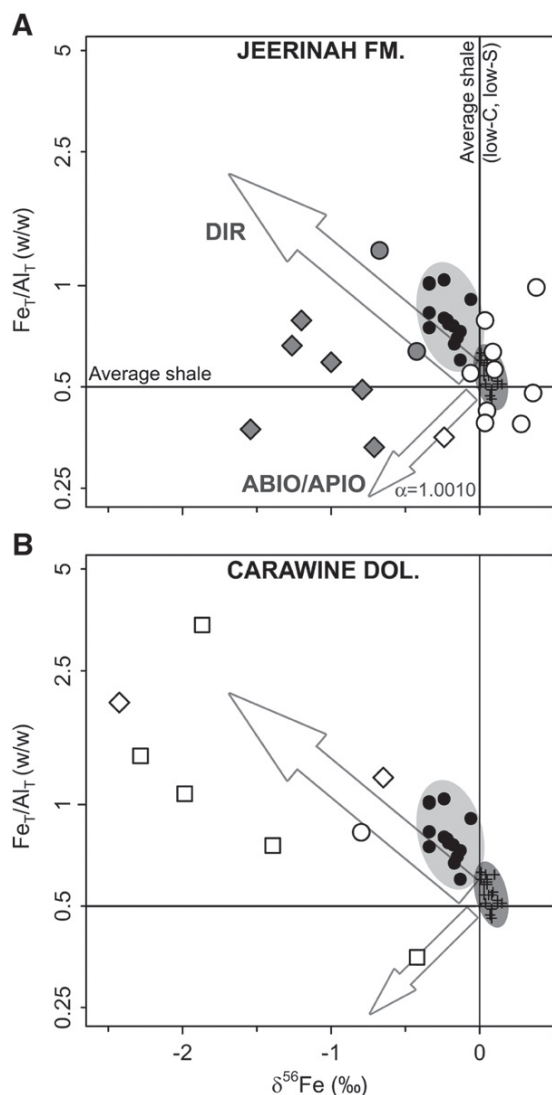
Fig. 5. Total Fe content of shales and carbonate-rich shales from the Jeerinah Formation (A) and the Carawine Dolomite (B), normalized to Al contents (Fe$_T$/Al$_T$), versus δ^{56}Fe values. For comparison, data for oxic (crosses in dark gray field) and euxinic (filled black circles in light gray field) sediments in the modern Black Sea (Severmann et al., 2008) are plotted. Symbols for Archean samples are the same as those in Fig. 3. The open arrows indicate the general directions of deviations from average shale values (denoted by the horizontal and vertical lines) caused by bacterial dissimilatory iron reduction (DIR), or oxidation of Fe$^{2+}_{aq}$ by abiological Rayleigh fractionation (ABIO) or anoxygenic photosynthetic iron oxidation (APIO). Note that data for the Wittenoom Formation are not plotted because carbonate contents are generally >50 wt.% (as CO$_3$), whereas the carbonate-rich shales of the Carawine Dolomite are included because they generally have <50 wt.% carbonate (as CO$_3$). The samples studied by Severmann et al. (2008) contain 20–45 wt.% carbonate (as CO$_3$).

Zerkle et al., 2005; Eigenbrode and Freeman, 2006; Hayes and Waldbauer, 2006; Olson, 2006; Eigenbrode et al., 2008). Below, we first briefly review the metabolic pathways that were likely involved in C, S, and Fe cycling in the Neoarchean Hamersley Province (Table 1), followed by a detailed discussion of the temporal trends.

4.1. Overview of microbial pathways

Photosynthetic fixation of CO$_2$ was undoubtedly the major source of organic carbon that fueled a large number of other metabolisms. Though still somewhat controversial, an increasing body of molecular
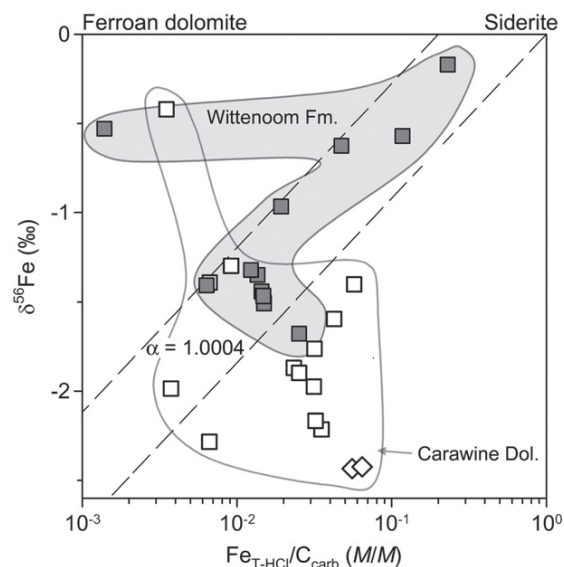
Fig. 6. δ^{56}Fe values for carbonates of the Wittenoom Formation (gray shaded area) and carbonate and carbonate-rich shales from the Carawine Dolomite (open outlined area) plotted against total HCl-extractable Fe, normalized by carbonate carbon content (M/M). On this scale, siderite would have a value of 1 (10^0) and ferroan dolomite would have a value of $\leq 10^{-1}$ (Deer et al., 1992). For reference, thin dashed lines show calculated Rayleigh fractionations assuming a fractionation factor of -0.4‰ between ferrous and ferric Fe precipitate, and initial Fe$_{T-HCl}$/C$_{carb}$ ratios of 0.2 (left) and 1.0 (right); this fractionation factor was arbitrarily chosen because many of the data from the Wittenoom Formation samples fit such a factor. Symbols are the same as those in Fig. 3.

biomarker work (e.g., Eigenbrode et al., 2008; Waldbauer et al., 2009) is confirming initial reports (e.g., Brocks et al., 1999) that oxygenic photosynthesis was established by the Neoarchean. Early photosynthesis likely included anoxygenic photosynthetic iron oxidation (APIO; Table 1) (e.g., Widdel et al., 1993; Canfield, 2005; Canfield et al., 2006; Olson, 2006). At circum-neutral pH, the Fe^{3+} produced by APIO (see Table 1) or by abiological reaction of Fe$^{2+}_{aq}$ with photosynthetically produced free O$_2$ reacts with water to form ferric oxide/hydroxide precipitates [e.g., Fe(OH)$_3$].

Iron and sulfur oxidation and production of organic carbon create the essential components required to support heterotrophic respiration, including bacterial dissimilatory iron reduction (DIR), and bacterial sulfate reduction (BSR) (Table 1). DIR is considered to be one of the earliest microbial metabolisms on Earth (Vargas et al., 1998; Lovley, 2004) and involves oxidation of organic carbon by the use of ferric iron minerals (ferric oxide/hydroxides) as electron

Table 1
Simplified metabolic reactions of Neoarchean sedimentary environments.

Metabolism	Reaction
Oxygenic photosynthesis	$CO_2 + H_2O \rightarrow CH_2O + O_2$
Anoxygenic photosynthetic iron oxidation (APIO)	$4Fe^{2+} + CO_2 + 4H^+ \rightarrow CH_2O + 4Fe^{3+} + H_2O$
Dissimilatory iron reduction (DIR)	$4Fe(OH)_3 + CH_2O \rightarrow 4Fe^{2+} + HCO_3^- + 7OH^- + 3H_2O$
Bacterial sulfate reduction (BSR)	$SO_4^{2-} + CH_2O \rightarrow 2HCO_3^- + H_2S$
Methanogenesis	$CO_2 + 4H_2 \rightarrow CH_4 + 2H_2O$ or $CH_3COOH \rightarrow CH_4 + CO_2$
Aerobic methanotrophy (AMT)	$7CH_4 + 8O_2 \rightarrow 6CH_2O + CO_2 + 8H_2O$
Anaerobic oxidation of methane	
Coupled to sulfate reduction (AOM-SR)	$CH_4 + SO_4^{2-} \rightarrow HCO_3^- + HS^- + H_2O$
Coupled to iron reduction (AOM-IR)	$CH_4 + 8Fe(OH)_3 + 15H^+ \rightarrow HCO_3 + 8Fe^{2+} + 21H_2O$

acceptors (e.g., Lovley, 2004). BSR is analogous to DIR, but uses sulfate (SO_4^{2-}) as an electron acceptor.

Below the photic zone, chemosynthetic organisms are the dominant carbon fixers and exist in a redox couple with fermentors and methylotrophs. Methanogenesis, likely a dominant anaerobic chemoautotrophic metabolism in the Neoarchean (Schidlowski et al., 1983; Eigenbrode et al., 2008), typically involves the use of CO_2 or acetic acid as an electron acceptor and produces CH_4 that has very low $\delta^{13}C$ values (Table 1). As proposed by Hayes (1983), and supported by molecular biomarker evidence (Eigenbrode et al., 2008), aerobic methanotrophy (AMT) is a possible metabolism in the Neoarchean that was associated with free O_2 in the ocean and would have utilized the CH_4 produced by methanogens (Table 1). In regard to Fe cycling, AMT would indicate the presence of free O_2, which would provide a means for oxidizing hydrothermal Fe^{2+}_{aq} to form ferric oxide/hydroxide precipitates, which, along with the organic C produced by AMT, in turn could support DIR.

Anaerobic oxidation of methane (AOM; Table 1) is another process that operates in modern marine sediments (e.g., Boetius et al., 2000; D'Hondt et al., 2004; Sivan et al., 2007) and could explain the highly negative $\delta^{13}C$ values for Neoarchean kerogen (e.g., Hinrichs, 2002). Today, this metabolism is most commonly coupled to sulfate reduction. Because AOM commonly operates in the zone of iron reduction in modern sediments (e.g., D'Hondt et al., 2004), it is possible that DIR and AOM occur together, but are not directly coupled. Recently, however, AOM has been shown to also be directly coupled to Fe and Mn reduction (Beal et al., 2009), which may have been important under conditions of high reactive Fe, but relatively low sulfate and Mn contents, as was likely characteristic of the Neoarchean Hamersley Province.

4.2. Temporal variations in C–Fe cycling in the Neoarchean Hamersley Province

We group our discussion into four sections: 1) the very shallow-water, mixed clastic deposition and carbonate precipitation (Tumbiana Formation), 2) variable but relatively deep-water deposition of pyritic black shale in the depocenter of the paleobasin, compared with relatively less deep-water deposition on the margin (Jeerinah Formation), 3) transition of the deep-water shale deposition to deep-water iron formation and shale deposition (Marra Mamba IF) in the center of the paleobasin, and coeval deposition of a relatively Fe-rich carbonate platform on the margin (Carawine Dolomite), and 4) variable but relatively shallow-water (photic zone) carbonate and clastic deposition (Fe-poor Wittenoom Formation).

4.2.1. Clastic/carbonate dominated Fe cycle

The very shallow-water deposits of the Tumbiana Formation have $\delta^{56}Fe$ values that are close to the crustal average ($\delta^{56}Fe \approx 0‰$). The near-zero $\delta^{56}Fe$ values, and the fact that the iron in these samples is predominantly in phyllosilicates (Table S2), indicate minimal Fe redox cycling. The relative paucity of Fe cycling is consistent with the relatively low reactive Fe contents (Table S2 and Fig. S3). Previously reported kerogen C isotope compositions from this unit have an average $\delta^{13}C_{ker}$ value of −46.1‰, interpreted to reflect the presence of organic carbon from methylotrophs (Table S2 and Fig. 4C; Eigenbrode and Freeman, 2006; Eigenbrode et al., 2008). Bottomley et al. (1992) and Thomazo et al. (2009) reported $\delta^{34}S$ values for samples from the Tumbiana Formation that suggest a component of BSR, although the small range of isotope fractionation ($\delta^{34}S = -5.73$ to $+2.75‰$) was interpreted to indicate biological cycling in a sulfate-limited environment.

4.2.2. Deep-water bacterial iron shuttle: the Jeerinah Formation

The Jeerinah Formation in the depocenter of the paleobasin (core WRL1) has a bulk composition indicative of euxinic (anoxic and sulfidic) conditions relative to the temporally equivalent rocks from the Oakover River area (core RHDH2a) (Figs. S3 and S4), and this contrast is reflected in markedly different Fe isotope trends (Fig. 4A). However, Richards (1985) noted significant pyrite in parts of the Jeerinah Formation of the Oakover River area and thus occasional euxinic conditions may have existed in this region. Fig. 7 schematically illustrates the Fe isotope and relative depositional settings for the two localities during Jeerinah Formation deposition, although it is important to note that sediments in each region of the province were deposited in relatively deep water, below storm wave base. The
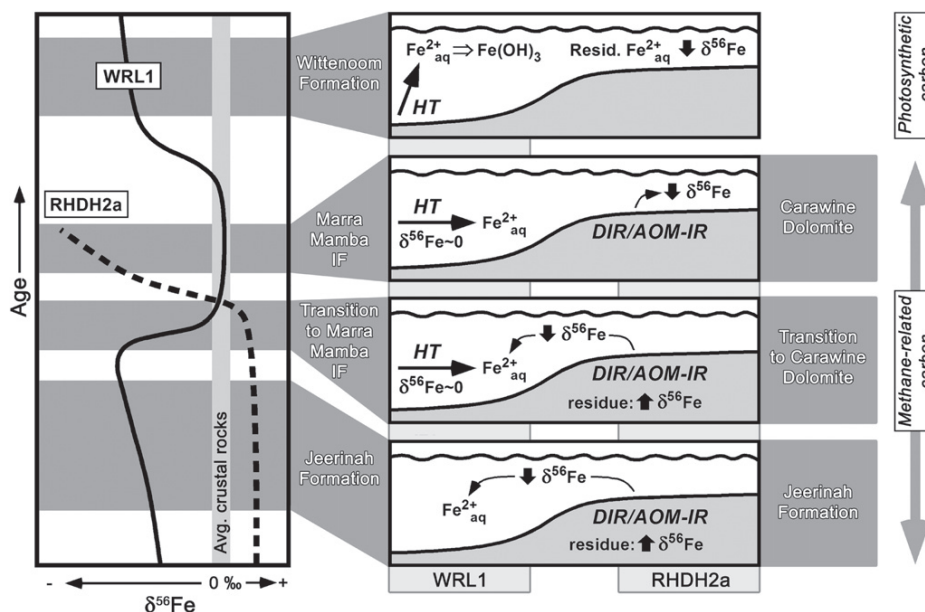
Fig. 7. Summary of measured Fe (left) and kerogen C (far right) isotope compositions for the Hamersley Province and schematic environmental interpretations for four time periods (center). See text for descriptions. The Fe isotope curves are schematically redrawn from the collected isotope data shown in Fig. 4A. In the center panels, heavy vertical arrows indicate increasing or decreasing $\delta^{56}Fe$ values. Dominant carbon sources are noted on the right based on average $\delta^{13}C_{ker}$ values. AOM-IR, anaerobic oxidation of methane coupled to iron reduction; DIR, dissimilatory iron reduction; HT, hydrothermal source.

relatively high Fe contents of the Jeerinah Formation (Fig. 4B) preclude production of the negative δ^{56}Fe values through extensive oxide precipitation. Instead, the negative δ^{56}Fe values that are found in samples collected from core WRL1 are interpreted to record transport, or "shuttling", of low-δ^{56}Fe Fe^{2+}_{aq} from the paleobasin margin to the euxinic depocenter in the main outcrop area, following the model proposed by Severmann et al. (2008), which built upon previous work (Anderson and Raiswell, 2004; Raiswell and Anderson, 2005; Lyons and Severmann, 2006; Severmann et al., 2006). Evidence for Fe "shuttling" is recorded in increases in Fe_T/Al_T ratios and decreases in δ^{56}Fe values for euxinic sediments of the Black Sea (Fig. 5). In this model, ferric Fe is reduced in the sediments on a shallow shelf by DIR, producing Fe^{2+}_{aq} that has a low δ^{56}Fe value, followed by transport to the deep euxinic Black Sea basin, where it is quantitatively sequestered through reaction with abundant H_2S, producing pyrite and retaining the low-δ^{56}Fe values of the DIR-generated Fe (Severmann et al., 2008). Presumably the driving mechanism for Fe shuttling is the concentration gradient imposed by the sulfide sink in the euxinic part of the basin. Other studies have interpreted low-δ^{56}Fe values to record DIR in modern and ancient marine sediments (Archer and Vance, 2006; Bergquist and Boyle, 2006; Staubwasser et al., 2006; Homoky et al., 2009), and in a lacustrine water column (Teutsch et al., 2009).

An important test of the basin Fe shuttle model is documenting the complementary high-δ^{56}Fe reservoir that is required by isotopic mass balance (Johnson et al., 2008b; Lyons et al., 2009), and Severmann et al. (2008) demonstrated that oxic shelf sediments in the Black Sea have slightly positive δ^{56}Fe values that may balance the negative δ^{56}Fe values in the euxinic deep-water sediments (see Fig. 5). Staubwasser et al. (2006) also found evidence for DIR in modern sediments from the shelf of the northeast Arabian Sea, in the form of low-δ^{56}Fe reactive Fe^{3+} and slightly positive δ^{56}Fe values of bulk Fe. In the Hamersley Province, we suggest that the high-δ^{56}Fe reservoir is provided by the Jeerinah Formation shales from the Oakover River area (core RHDH2a; Figs. 4A and 7), although we note that the regions of the Hamersley Province sampled in this study are separated by ~300 km and likely by a topographic high in the Neoarchean (Morris, 1993). Thus, we do not claim that Fe was shuttled from one region to the other, but rather that the main outcrop area represents a region where low-δ^{56}Fe Fe^{2+}_{aq} was sequestered and the Oakover River area was one from which low-δ^{56}Fe Fe^{2+}_{aq} was removed. Although the correlation between Fe_T/Al_T ratios and δ^{56}Fe values for the Jeerinah Formation samples is not as strong as that for the modern Black Sea samples (Fig. 5A), the key observation relevant to a DIR-driven shuttle is that there is a large reservoir of low-δ^{56}Fe Fe in the deeper, euxinic

part of the paleobasin that is contemporaneous with a slightly positive δ^{56}Fe reservoir in the relatively shallower part of the paleobasin. Additionally, abiologic Fe^{2+}_{aq} oxidation would produce large quantities of ferric oxides in the Jeerinah Formation of the Oakover River area, which is inconsistent with our data (Table S2 and Fig. 4).

Severmann et al. (2008) postulate on several aspects of an Archean Fe shuttle, but our results, when combined with C and S isotope data, and consideration of the range of microbial metabolisms that operated in the paleobasins of the Hamersley Province, provide a broader view of the Fe shuttle model in the Archean (Fig. 8). First, the slightly negative to positive δ^{34}S values that typify sulfides in the 2.7 to 2.5 Ga Hamersley Province samples (Bottomley et al., 1992; Yamaguchi, 2002; Ono et al., 2003; Partridge et al., 2008; Thomazo et al., 2009) suggest moderate to strong sulfate limitation during BSR, which in turn suggests that seawater sulfide contents were lower than those of the Black Sea (Fig. 8). This issue was recognized by Severmann et al. (2008), who proposed that because of limited sulfate and excess Fe^{2+}_{aq} in the Archean, the δ^{56}Fe values of precipitated pyrite in the rock record could be as much as ~1.5‰ lower than the Fe^{2+}_{aq} source, although it is possible that the δ^{56}Fe values of pyrite will directly reflect those of precursor Fe-S minerals and fluids (Butler et al., 2005).

The highly negative δ^{13}C values of kerogen in Neoarchean marine sedimentary rocks (e.g., Fig. 4C) indicate that a wide variety of methane-related pathways must also be considered, and in this regard there are similarities between the Hamersley Province paleobasin and the modern Black Sea (Fig. 8); note, however, that in both environments, highly negative $\delta^{13}C_{ker}$ values indicate a mix of photosynthetically generated C ($\delta^{13}C \approx$ -30‰) and methanogen-generated C ($\delta^{13}C <$ -60‰) (e.g., Freeman et al., 1994; Eigenbrode and Freeman, 2006; Eigenbrode et al., 2008). Aerobic methanotrophy (AMT) occurs in the water column of the Black Sea today, at the oxic/anoxic transition, in the same zone as DIR (e.g., Blumenberg et al., 2007; Wakeham et al., 2007), suggesting that AMT in the Hamersley Province paleobasin could have occurred under relatively low O_2 conditions (Fig. 8). In addition to anaerobic oxidation of methane coupled to sulfate reduction (AOM-SR; Fig. 8), AOM coupled to iron reduction (AOM-IR) could have occurred in suboxic zones of the paleobasin. We speculate that the Fe isotope fractionations produced by AOM-IR should be similar to those produced by DIR, where low-δ^{56}Fe values for Fe^{2+}_{aq} would reflect isotopic exchange with high-δ^{56}Fe surface Fe^{3+} on iron oxide/hydroxides (Crosby et al., 2005, 2007). Although it is plausible that AOM-IR produced the negative δ^{56}Fe and δ^{13}C values in the Jeerinah Formation (Fig. 4C and Fig. S5F), it is also possible that this relation is coincidental, where Fe isotope
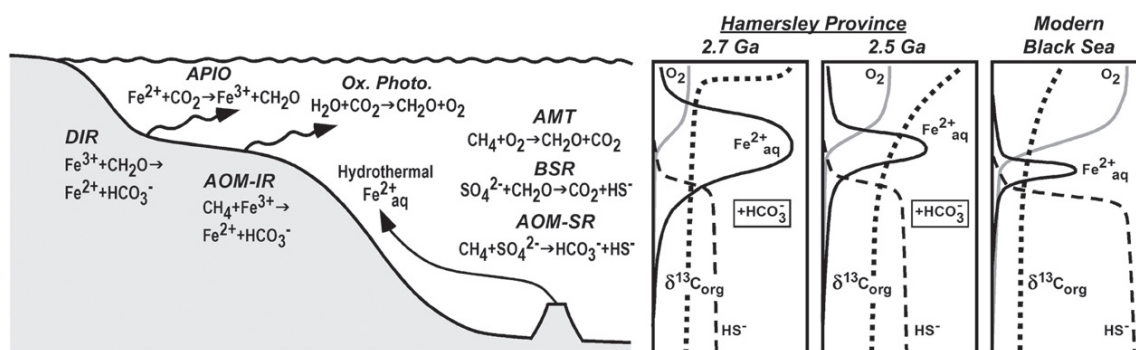
Fig. 8. Schematic diagram of a basin water column illustrating the microbial metabolisms discussed in the text, put into simplified environmental context (left), and interpretive water column depth profiles of various chemical constituents of the Hamersley Province and the modern Black Sea (right). Chemical reactions are simplified and not intended to be balanced. AMT, aerobic methanotrophy; AOM-IR, anaerobic oxidation of methane coupled to iron reduction; AOM-SR, anaerobic oxidation of methane coupled to sulfate reduction; APIO, anoxygenic photosynthetic iron oxidation; BSR, bacterial sulfate reduction; DIR, dissimilatory iron reduction; Ox. Photo, oxygenic photosynthesis. Note that although AMT, BSR, and AOM-SR reactions are placed in the water column in the diagram, these may also occur in the sediment. APIO and oxygenic photosynthesis are photic-zone metabolisms and would thus occur in the shallow-water column. Schematic water column profiles are shown for changing conditions in the Hamersley Province from 2.7 to 2.5 Ga. Several aspects of the figure draw from those of Severmann et al. (2008).

fractionations were generated by DIR, but C isotope fractionations reflect AMT and AOM in the same sediment. The association of highly negative $\delta^{13}C_{ker}$ values with negative $\delta^{56}Fe$ values, therefore, may simply reflect the large zone of suboxic diagenesis that would be associated with methane cycling. We propose that such a zone would produce a large vertical interval of high-Fe^{2+}_{aq} contents, relative to the more restricted oxic/anoxic transitions in modern environments such as the Black Sea (Fig. 8).

4.2.3. Early Hamersley Province iron formation and ferroan carbonates

The increase in $\delta^{56}Fe$ values for Marra Mamba Iron Formation shales immediately above the Jeerinah Formation is interpreted to record a major shift in Fe sources to the deeper portion of the Hamersley Province toward near-zero hydrothermal Fe, and concomitant decreases in DIR-driven Fe shuttling (Fig. 7). This is consistent with the high Fe fluxes that are required in BIF depositional models (Klein, 2005). It is important to stress that the Marra Mamba IF samples analyzed in this study are shales, and therefore reflect a mixture of clastic and hydrothermal Fe, but both sources should have had $\delta^{56}Fe$ values near zero, and this is recorded in the samples analyzed from the main section of the iron formation (Figs. 4A and 7).

During deposition of the Marra Mamba IF in the main part of the province, deposition of the Carawine Dolomite in the Oakover River area on the margin of the province was accompanied by a very large decrease in $\delta^{56}Fe$ values (Figs. 4A and 7). The near-zero $\delta^{13}C$ values for carbonate of the Carawine Dolomite (Fig. 4C) indicate equilibrium with seawater, suggesting the $\delta^{56}Fe$ values of the carbonate-bearing shales analyzed in this study at least in part reflect those of seawater. The correlations of increasing Fe_T/Al_T contents and somewhat increasing Fe_{T-HCL}/C_{carb} contents with decreasing $\delta^{56}Fe$ values are opposite that expected for oxidation of Fe^{2+}_{aq} (Figs. 5B and 6). We interpret this relation to indicate generation of low-$\delta^{56}Fe$ Fe^{2+}_{aq} through DIR and transport via an Fe shuttle, although one that operated on a localized scale, between open water suboxic and restricted anoxic/euxinic environments (Fig. 7). This interpretation is consistent with the observation that Fe contents of the Carawine Dolomite are higher than those of Archean shelf carbonates (Fig. 4B), and opposite the relations predicted by extensive Fe^{2+} oxidation, which would produce very low Fe contents in the carbonates. The Fe budget of the carbonate-rich shales of the Carawine Dolomite varies from ferroan dolomite- to pyrite-dominated, and highly negative $\delta^{56}Fe$ values are found in both types of samples. To the degree that sulfide contents in the Hamersley Province were moderately low (Fig. 8), an important modification of the Fe shuttle model for the Archean is that the "trap" for mobilized Fe may include carbonate, in addition to sulfide. As is the case for sulfides (see Section 4.2.2), it is difficult to predict the exact $\delta^{56}Fe$ values of the resulting Fe-carbonates. Experimentally determined Fe isotope fractionation factors between Fe^{2+}_{aq} and carbonates are slightly positive (Wiesli et al., 2004), which suggests that the $\delta^{56}Fe$ values for precipitated carbonates would range from those equal to that of the Fe^{2+}_{aq} source if complete sequestration into carbonate occurred, or slightly lower than that of the Fe^{2+}_{aq} if precipitation occurred under equilibrium conditions.

Samples from the restricted environments of the Carawine Dolomite carbonate platform record the lowest $\delta^{56}Fe$ values measured here as well as some of the lowest $\delta^{13}C_{ker}$ values, whereas samples from non-restricted platform environments record relatively less negative $\delta^{56}Fe$ and $\delta^{13}C_{ker}$ values (Fig. S5G). This relation suggests that in restricted settings, where DIR-produced low-$\delta^{56}Fe$ Fe^{2+}_{aq} was trapped as ferroan dolomite or pyrite, anoxia allowed an increased contribution of methane-related metabolisms relative to the suboxic open water environments.

4.2.4. Photic-zone Fe oxidation

The Wittenoom Formation was deposited in water below storm wave base, but it is interpreted to largely record processes that occurred in the shallow photic zone of the Neoarchean Hamersley

Province (see Supplementary material online). In addition, because $\delta^{13}C$ values of kerogens from the Wittenoom Formation are significantly higher than those of older units (Table S2 and Fig. 4C), Eigenbrode and Freeman (2006) interpreted the measured $\delta^{13}C_{ker}$ values to largely reflect C fixation by photosynthesis in shallow-water environments. The moderately negative $\delta^{13}C_{ker}$ values of $\sim -30‰$ in the Wittenoom Formation (Table S2) could be the product of either oxygenic photosynthesis or APIO, given the generally similar C isotope fractionations for different photosynthetic pathways (e.g., Zerkle et al., 2005); support for oxygenic photosynthesis comes from high abundances of 2α-methylhopanes in shallow-water facies of the Hamersley Province (Eigenbrode et al., 2008). Konhauser et al. (2009) suggest that the overall increase in $\delta^{13}C_{ker}$ values in the Neoarchean is due to a decrease in methanogen abundance caused by depletion in oceanic nickel, an important metal co-factor in several methanogen enzymes. The significantly negative $\delta^{34}S$ values for pyrite nodules in the Wittenoom Formation indicate BSR in the presence of excess sulfate (Partridge et al., 2008), which suggests relatively high levels of O_2 in at least the upper water column, consistent with temporal S isotope (Bottomley et al., 1992; Yamaguchi, 2002; Ono et al., 2003; Kaufman et al., 2007) and N isotope (Godfrey and Falkowski, 2009) trends. The near-zero $\delta^{13}C$ values for carbonates of the Wittenoom Formation (Fig. 4C) suggest that these units formed in equilibrium with seawater.

The strong correlation of decreasing $\delta^{56}Fe$ values with decreasing Fe contents relative to carbonate (Fig. 6) for the Wittenoom Formation is exactly that predicted by oxidation of Fe^{2+}_{aq} in the photic zone of the Hamersley Province, accompanied by precipitation of ferric oxide/hydroxides, producing low-$\delta^{56}Fe$ values in the remaining Fe^{2+}_{aq} via a Rayleigh process (Fig. 7), essentially the model proposed by Rouxel et al. (2005) and Anbar and Rouxel (2007). Oxidation of Fe^{2+}_{aq} could reflect an indirectly biological mechanism, such as oxidation by photosynthetically generated O_2, or a directly biological process such as APIO (see Table 1), which also produces low-$\delta^{56}Fe$ values in the residual Fe^{2+}_{aq} (Bullen et al., 2001; Croal et al., 2004). The low $\delta^{56}Fe$ values measured in the Wittenoom Formation therefore reflect incorporation of a low-$\delta^{56}Fe$ Fe^{2+}_{aq} pool that remains after extensive oxide precipitation, where the $\delta^{56}Fe$ values either directly record the isotopic composition of Fe^{2+}_{aq} if complete sequestration occurs or slightly lower $\delta^{56}Fe$ values if formation occurred under equilibrium conditions using the Fe^{2+}_{aq}–carbonate fractionation factor of Wiesli et al. (2004).

5. Conclusions

The approximately contemporaneous large negative excursions in kerogen $\delta^{13}C$ values and bulk/mineral $\delta^{56}Fe$ values in the Neoarchean marine sedimentary rock record can be explained by environmental controls on C and Fe cycles that were imposed directly or indirectly by the likely microbial metabolisms operating at that time, although the diversity of C and Fe metabolisms does not predict that C and Fe isotopes should always be correlated. Direct coupling of methane cycling with microbial Fe redox cycling could have occurred through anaerobic oxidation of methane coupled to Fe reduction (AOM-IR). Methane and Fe cycling could have been indirectly coupled via aerobic methanotrophy (AMT), where the required free O_2 could have oxidized hydrothermal Fe^{2+}, which, when coupled to the organic carbon produced by AMT, could have supported dissimilatory iron reduction (DIR). Independent support for AMT comes from molecular biomarker studies of the same samples as analyzed here. Anaerobic oxidation of methane coupled to sulfate reduction (AOM-SR) may have been limited during at least the early history of the Hamersley Province, given the narrow range in $\delta^{34}S$ values determined in numerous studies on samples similar to those studied here, which suggests limited seawater sulfate. The increase in $\delta^{13}C$ values for kerogen and $\delta^{56}Fe$–Fe content relations in younger samples, as well as

molecular biomarker studies, suggest an increase in oxygenic photosynthetic contributions to C cycling and Fe redox cycling by oxide precipitation through reaction of Fe^{2+}_{aq} with photosynthetically generated O_2.

Across-province comparison of the Jeerinah Formation provides evidence for a basin Fe shuttle generated by DIR, where low-$\delta^{56}Fe$ Fe^{2+}_{aq} was lost from suboxic zones on the margin and trapped in the euxinic portions of the central part of the paleobasin, the first clear Archean example of the model proposed by Severmann et al. (2008) for the modern Black Sea. Younger deep-water shales from the center of the province, deposited along with banded iron formation (Marra Mamba IF), record an increase in Fe input from hydrothermal and clastic sources as recorded by near-zero $\delta^{56}Fe$ values. On the margin of the province, shallow-water mixed carbonate/shale lithologies of the Carawine Dolomite record the lowest $\delta^{56}Fe$ values measured in this study. The negative correlation between $\delta^{56}Fe$ values and Fe contents in these deposits indicates a likely role for DIR in this environment, and suggests that carbonates, in low-sulfide environments, may also "trap" low-$\delta^{56}Fe$ Fe^{2+}_{aq} during DIR-driven Fe shuttling. In contrast, the youngest samples studied here, the shallow-water carbonates of the Wittenoom Formation, record photic-zone processes, as indicated by their relatively high $\delta^{13}C$ values for kerogen. Samples from this unit have $\delta^{56}Fe$ values that decrease exponentially with Fe contents, a pattern that reflects Rayleigh fractionation during Fe^{2+}_{aq} oxidation by O_2 in the water column. Our study demonstrates that controversial interpretations of the Fe isotope record in Neoarchean and Paleoproterozoic sediments may be reconciled through detailed, basin-scale studies, and both extensive oxidation and DIR-driven redox cycling may occur in the same basin.

Acknowledgements

Appendix A. Supplementary data

Supplementary data associated with this article can be found, in the online version, at doi:10.1016/j.epsl.2010.01.032.

References

Albarède, F., Beard, B.L., 2004. Analytical methods for non-traditional isotopes. In: Johnson, C.M., Beard, B.L., Albarède, F. (Eds.), Geochemistry of Non-Traditional Stable Isotopes, Reviews in Mineralogy & Geochemistry. : Mineralogical Society of America and Geochemical Society, 55. Washington, DC, pp. 113–152.

Anbar, A.D., Jarzecki, A.A., Spiro, T.G., 2005. Theoretical investigation of iron isotope fractionation between $Fe(H_2O)_6^{3+}$ and $Fe(H_2O)_6^{2+}$: implications for iron stable isotope geochemistry. Geochim. Cosmochim. Acta 69, 825–837.

Anbar, A.D., Rouxel, O., 2007. Metal stable isotopes in paleoceanography. Annu. Rev. Earth Planet. Sci. 35, 717–746.

Anderson, T.F., Raiswell, R., 2004. Sources and mechanisms for the enrichment of highly reactive iron in euxinic Black Sea sediments. Am. J. Sci. 304, 203–233.

Archer, C., Vance, D., 2006. Coupled Fe and S isotope evidence for Archean microbial Fe (III) and sulfate reduction. Geology 34, 153–156.

Arndt, N.T., Nelson, D.R., Compston, W., Trendall, A.F., Thorne, A.M., 1991. The age of the Fortescue Group, Hamersley basin, Western Australia, from ion microprobe zircon U–Pb results. Aust. J. Earth Sci. 38, 261–281.

Battistuzzi, F.U., Feijao, A., Hedges, S.B., 2004. A genomic timescale of prokaryote evolution: insights into the origin of methanogenesis, phototrophy, and the colonization of land. BMC Evol. Biol. 4, 44.

Beal, E.J., House, C.H., Orphan, V.J., 2009. Manganese- and iron-dependent marine methane oxidation. Science 325, 184–187.

Beard, B.L., Johnson, C.M., Skulan, J.L., Nealson, K.H., Cox, L., Sun, H., 2003. Application of Fe isotopes to tracing the geochemical and biological cycling of Fe. Chem. Geol. 195, 87–117.

Bergquist, B.A., Boyle, E.A., 2006. Iron isotopes in the Amazon River system: weathering and transport signatures. Earth Planet. Sci. Lett. 248, 54–68.

Blake, T.S., 1993. Late Archean crustal extension, sedimentary basin formation, flood basalt volcanism and continental rifting: the Nullagine and Mount Jope Supersequences, Western Australia. Precambrian Res. 60, 185–241.

Blake, T.S., Barley, M.E., 1992. Tectonic evolution of the Late Archean to Early Proterozoic Mount Bruce Megasequence Set, Western Australia. Tectonics 11, 1415–1425.

Blake, T.S., Buick, R., Brown, S.J.A., Barley, M.E., 2004. Geochronology of a Late Archaean flood basalt province in the Pilbara Craton, Australia: constraints on basin evolution, volcanic and sedimentary accumulation, and continental drift rates. Precambrian Res. 133, 143–173.

Blockley, J.G., Tehnas, I.J., Mandyczewsky, A., Morris, R.C., 1993. Proposed stratigraphic subdivisions of the Marra Mamba Iron Formation and the lower Wittenoom Dolomite, Hamersley Group, Western Australia. Geol. Surv. West. Aust. Report 34, 47–63.

Blumenberg, M., Seifert, R., Michaelis, W., 2007. Aerobic methanotrophy in the oxic–anoxic transition zone of the Black Sea water column. Org. Geochem. 38, 84–91.

Boetius, A., Ravenschlag, K., Schubert, C.J., Rickert, D., Widdel, F., Gieseke, A., Amann, R., Jorgensen, B.B., Witte, U., Pfannkuche, O., 2000. A marine microbial consortium apparently mediating anaerobic oxidation of methane. Nature 407, 623–626.

Bottomley, D.J., Veizer, J., Nielsen, H., Moczydlowska, M., 1992. Isotopic composition of disseminated sulfur in Precambrian sedimentary rocks. Geochim. Cosmochim. Acta 56, 3311–3322.

Brocks, J.J., Logan, G.A., Buick, R., Summons, R.E., 1999. Archean molecular fossils and the early rise of eukaryotes. Science 285, 1033–1036.

Bullen, T.D., White, A.F., Childs, C.W., Vivit, D.V., Schulz, M.S., 2001. Demonstration of significant abiotic iron isotope fractionation in nature. Geology 29, 699–702.

Butler, I.B., Archer, C., Vance, D., Oldroyd, A., Rickard, D., 2005. Fe isotope fractionation on FeS formation in ambient aqueous solution. Earth Planet. Sci. Lett. 236, 430–442.

Canfield, D.E., 2005. The early history of atmospheric oxygen: homage to Robert Garrels. Annu. Rev. Earth Planet. Sci. 33, 1–36.

Canfield, D.E., 2001. Isotope fractionation by natural populations of sulfate-reducing bacteria. Geochim. Cosmochim. Acta 65, 1117–1124.

Canfield, D.E., Raiswell, R., 1999. The evolution of the sulfur cycle. Am. J. Sci. 299, 697–723.

Canfield, D.E., Rosing, M.T., Bjerrum, C., 2006. Early anaerobic metabolisms. Phil. Trans. R. Soc. B 361, 1819–1836.

Canfield, D.E., Teske, A., 1995. Late Proterozoic rise in atmospheric oxygen concentration inferred from phylogenetic and sulfur-isotope studies. Nature 382, 127–132.

Croal, L.R., Johnson, C.M., Beard, B.L., Newman, D.K., 2004. Iron isotope fractionation by Fe(II)-oxidizing photoautotrophic bacteria. Geochim. Cosmochim. Acta 68, 1227–1242.

Crosby, H.A., Johnson, C.M., Roden, E.E., Beard, B.L., 2005. Coupled Fe(II)–Fe(III) electron and atom exchange as a mechanism for Fe isotope fractionation during dissimilatory iron oxide reduction. Environ. Sci. Technol. 39, 6698–6704.

Crosby, H.A., Roden, E.E., Johnson, C.M., Beard, B.L., 2007. The mechanisms of iron isotope fractionation produced during dissimilatory Fe(III) reduction by Shewanella putrefaciens and Geobacter sulfurreducens. Geobiology 5, 169–189.

Dauphas, N., van Zuilen, M., Wadhwa, M., Davic, A.M., Marty, B., Janney, P.E., 2004. Clues from Fe isotope variations on the origin of Early Archean BIFs from Greenland. Science 306, 2077–2080.

Deer, W.A., Howie, R.A., Zussman, J., 1992. An Introduction to the Rock-Forming Minerals, second ed. Prentice Hall, Harlow, England.

D'Hondt, S., Joergensen, B.B., Miller, D.J., Batzke, A., Blake, R., Cragg, B.A., Cypionka, H., Dickens, G.R., Ferdelman, T., Hinrichs, K., Holm, N.G., Mitterer, R., Spivack, A., Wang, G., Bekins, B., Engelen, B., Ford, K., Gettemy, G., Rutherford, S.D., Sass, H., Skilbeck, C.G., Aiello, I.W., Guerin, G., House, C.H., Inagaki, F., Meister, P., Naehr, T., Niitsuma, S., Parkes, R.J., Schippers, A., Smith, D.C., Teske, A., Wiegel, J., Naranjo Padilla, C., Solis Acosta, J.L., 2004. Distributions of microbial activities in deep subseafloor sediments. Science 306, 2216–2221.

Eigenbrode, J.L., Freeman, K.H., 2006. Late Archean rise of aerobic microbial ecosystems. Proc. Natl. Acad. Sci. U. S. A. 103, 15759–15764.

Eigenbrode, J.L., Freeman, K.H., Summons, R.E., 2008. Methylhopane biomarker hydrocarbons in Hamersley Province sediments provide evidence for Neoarchean aerobiosis. Earth Planet. Sci. Lett. 273, 323–331.

Farquhar, J., Wing, B.A., 2003. Multiple sulfur isotopes and the evolution of the atmosphere. Earth Planet. Sci. Lett. 213, 1–13.

Freeman, K.H., Wakeham, S.G., Hayes, J.M., 1994. Predictive isotopic biogeochemistry: hydrocarbons from two anoxic marine basins. Org. Geochem. 21, 629–644.

Godfrey, L.V., Falkowski, P.G., 2009. The cycling and redox state of nitrogen in the Archean ocean. Nat. Geosci. 2, 725–729.

Hassler, S.W., Simonson, B.M., Sumner, D.Y., Murphy, M., 2005. Neoarchaean impact spherule layers in the Fortescue and Hamersley Groups, Western Australia: stratigraphic and depositional implications of re-correlation. Aust. J. Earth Sci. 52, 759–771.

Hayes, J.M., 1983. Geochemical evidence bearing on the origin of aerobiosis, a speculative hypothesis. In: Schopf, J.W. (Ed.), Earth's Earliest Biosphere. Its Origin and Evolution. Princeton University Press, Princeton, NJ, pp. 291–301.

Hayes, J.M., Waldbauer, J.R., 2006. The carbon cycle and associated redox processes through time. Phil. Trans. R. Soc. B. 361, 931–950.

Hill, P.S., Schauble, E.A., Shahar, A., Tonui, E., Young, E.D., 2009. Experimental studies of equilibrium iron isotope fractionation in ferric aquo-chloro complexes. Geochim. Cosmochim. Acta 73, 2366–2381.

Hinrichs, K., 2002. Microbial Fixation of Methane Carbon at 2.7 Ga; was an Anaerobic Mechanism Possible? G3, p. 3. doi:10.1029/2001GC000286.

Homoky, W.B., Severmann, S., Mills, R.A., Statham, P.J., Fones, G.R., 2009. Pore-fluid Fe isotopes reflect the extent of benthic Fe redox recycling: evidence from continental shelf and deep-sea sediments. Geology 37, 751–754.

Johnson, C.M., Beard, B.L., 2006. Fe isotopes: an emerging technique for understanding modern and ancient biogeochemical cycles. GSA Today 16, 4–10.

Johnson, C.M., Beard, B.L., Klein, C., Beukes, N.J., Roden, E.E., 2008a. Iron isotopes constrain biologic and abiologic processes in banded iron formation genesis. Geochim. Cosmochim. Acta 72, 151–169.

Johnson, C.M., Beard, B.L., Roden, E.E., 2008b. The iron isotope fingerprints of redox and biogeochemical cycling in the modern and ancient Earth. Annu. Rev. Earth Planet. Sci. 36, 457–493.

Kaufman, A.J., Johnston, D.T., Farquhar, J., Masterson, A.L., Lyons, T.W., Bates, S., Anbar, A.D., Arnold, G.L., Garvin, J., Buick, R., 2007. Late Archean biospheric oxygenation and atmospheric evolution. Science 317, 1900–1903.

Klein, C., 2005. Some Precambrian banded iron-formations (BIFs) from around the world: their age, geologic setting, mineralogy, geochemistry, and origin. Am. Miner. 90, 1473–1499.

Konhauser, K.O., Pecoits, E., Lalonde, S.V., Papineau, D., Nisbet, E.G., Barley, M.E., Arndt, N.T., Zahnle, K., Kamber, B.S., 2009. Oceanic nickel depletion and a methanogen famine before the Great Oxidation Event. Nature 458, 750–753.

Kopp, R.E., Kirschvink, J.L., Hilburn, I.A., Nash, C.Z., 2005. The Paleoproterozoic snowball Earth: a climate disaster triggered by the evolution of oxygenic photosynthesis. Proc. Natl. Acad. Sci. U. S. A. 32, 11131–11136.

Lascelles, D.F., 2000. Marra Mamba iron formation stratigraphy in the eastern Chichester range, Western Australia. Aust. J. Earth Sci. 47, 799–806.

Lawrence, S.D., 1985. CRA Explration Pty. Ltd. final report on exploration completed within exploration license EL 47/104, Billadunna Spring, Pyramid, Western Australia. Item 3189. Western Australia Geological Survey open file.

Lovley, D.R., 2004. Potential role of dissimilatory iron reduction in the early evolution of microbial respiration. In: Seckbach, J. (Ed.), Origins, Evolution, and Biodiversity of Microbial Life. Kluwer, Amsterdam, pp. 301–313.

Lyons, T.W., Anbar, A.D., Severmann, S., Scott, C., Gill, B.C., 2009. Tracking euxinia in the ancient ocean: a multiproxy perspective and Proterozoic case study. Annu. Rev. Earth Planet. Sci. 37, 507–534.

Lyons, T.W., Severmann, S., 2006. A critical look at iron paleoredox proxies: new insights from modern euxinic marine basins. Geochim. Cosmochim. Acta. 70, 5698–5722.

Meakins, A.L., 1987. CRA Exploration Pty. Ltd. final report on exploration completed within the Mulga Project area, Mt. Bruce 1:250 000 sheet, Pilbara region, Western Australia. Item 3458. Western Australia Geological Survey open file.

Morris, R.C., 1993. Genetic modelling for banded iron-formation of the Hamersley Group, Pilbara Craton, Western Australia; Archaean and early Proterozoic geology of the Pilbara region, Western Australia. Precambrian Res. 60, 243–286.

Nelson, D.R., 2001. Compilation of Geochronology Data 2000: Geol. Surv. West. Aust. Rec. . 2001/2.

Ochman, H., Wilson, A.C., 1987. Evolution in bacteria: evidence for a universal substitution rate in cellular genomes. J. Mol. Evol. 26, 74–86.

Olson, J.M., 2006. Photosynthesis in the Archean Era. Photosynth. Res. 88, 109–117.

Ono, S., Eigenbrode, J.L., Pavlov, A.A., Kharecha, P., Rumble III, D., Kasting, J.F., Freeman, K.H., 2003. New insights into Archean sulfur cycle from mass-independent sulfur isotope records from the Hamersley Basin, Australia. Earth Planet. Sci. Lett. 213, 15–30.

Partridge, M.A., Golding, S.D., Baublys, K.A., Young, E., 2008. Pyrite paragenesis and multiple sulfur isotope distribution in late Archean and early Paleoproterozoic Hamersley Basin sediments. Earth Planet. Sci. Lett. 272, 41–49.

Polyakov, V.B., Mineev, S.D., 2000. The use of Mössbauer spectroscopy in stable isotope geochemistry. Geochim. Cosmochim. Acta 64, 849–865.

Raiswell, R., Anderson, T.F., 2005. Reactive iron enrichment in sediments deposited beneath euxinic bottom waters: constraints on supply by shelf recycling. In: McDonald, I., Boyce, A.J., Butler, I.B., Herrington, R.J., Polya, D.A. (Eds.), Mineral Deposits and Earth EvolutionGeological Society, London, Special Publication 248. Geological Society, London, pp. 179–194.

Rasmussen, B., Blake, T.S., Fletcher, I.R., 2005. U–Pb zircon age constraints on the Hamersley spherule beds: evidence for a single 2.63 Ga Jeerinah–Carawine impact ejecta layer. Geology 33, 725–728.

Richards, M.N., 1985. CRA Exploration Pty. Ltd. final report on exploration completed within exploration licenses Ripon Hills North 45/63, Ripon Hills South 45/64 and Gingarrigan Creek 45/65, Nullagine, S F 51-5, Western Australia. Item 2655. Western Australia Geological Survey open file.

Rosing, M.T., Frei, R., 2004. U-rich Archaean sea-floor sediments from Greenland—indications of >3700 Ma oxygenic photosynthesis. Earth Planet. Sci. Lett. 217, 237–244.

Rouxel, O.J., Bekker, A., Edwards, K.J., 2005. Iron isotope constraints on the Archean and Paleoproterozoic ocean redox state. Science 307, 1088–1091.

Schauble, E.A., Rossman, G.R., Taylor, H.P., 2001. Theoretical estimates of equilibrium Fe-isotope fractionations from vibrational spectroscopy. Geochim. Cosmochim. Acta 65, 2487–2497.

Schidlowski, M., 2001. Carbon isotopes as biogeochemical recorders of life over 3.8 Ga of Earth history: evolution of a concept. Precambrian Res. 106, 117–134.

Schidlowski, M., Hayes, J.M., Kaplan, I.R., 1983. Isotopic inferences of ancient biochemistries: carbon, sulfur, hydrogen, and nitrogen. In: Schopf, J.W. (Ed.), Earth's Earliest Biosphere, Its Origin and Evolution. Princeton University Press, Princeton, NJ, pp. 149–186.

Severmann, S., Johnson, C.M., Beard, B.L., McManus, J., 2006. The effect of early diagenesis on the Fe isotope compositions of porewaters and authigenic minerals in continental margin sediments. Geochim. Cosmochim. Acta 70, 2006–2022.

Severmann, S., Lyons, T.W., Anbar, A., McManus, J., Gordon, G., 2008. Modern iron isotope perspective on the benthic iron shuttle and the redox evolution of ancient oceans. Geology 36, 487–490.

Sheridan, P.P., Freeman, K.H., Brenchley, J.E., 2003. Estimated minimal divergence times of the major bacterial and archaeal phyla. Geomicrobiol. J. 20, 1–14.

Simonson, B.M., Schubel, K.A., Hassler, S.W., 1993. Carbonate sedimentology of the Early Precambrian Hamersley Group of Western-Australia. Precambrian Res. 60, 287–335.

Sivan, O., Schrag, D.P., Murray, R.W., 2007. Rates of methanogenesis and methanotrophy in deep-sea sediments. Geobiology 5, 141–151.

Smith, R.E., Perdrix, J.L., Parks, T.C., 1982. Burial metamorphism in the Hamersley Basin, Western Australia. J. Petrol. 23, 75–102.

Staubwasser, M., von Blanckenburg, F., Schoenberg, R., 2006. Iron isotopes in the early marine diagenetic iron cycle. Geology 34, 629–632.

Taylor, S.R., McLennan, S.M., 1985. The Continental Crust: its Composition and Evolution. Blackwell Scientific Publications, Oxford.

Teutsch, N., Schmid, M., Müller, B., Halliday, A.N., Bürgmann, H., Wehrli, B., 2009. Large iron isotope fractionation at the oxic–anoxic boundary in Lake Nyos. Earth Planet. Sci. Lett. 285, 52–60.

Thomazo, C., Ader, M., Farquhar, J., Philippot, P., 2009. Methanotrophs regulated atmospheric sulfur isotope anomalies during the Mesoarchean (Tumbiana Formation, Western Australia). Earth Planet. Sci. Lett. 279, 65–75.

Thorne, A.M., Trendall, A.F., 2001. Geology of the Fortescue Group, Pilbara Craton, Western Australia. Geological Survey of Western Australia: Bulletin, 144. 249 pp.

Trendall, A.F., Blockley, J.G., 1970. The iron formations of the Precambrian Hamersley Group, Western Australia. Geological Survey of Western Australia: Bulletin, 119. 366 pp.

Trendall, A.F., Compston, W., Nelson, D.R., De Laeter, J.R., Bennett, V.C., 2004. SHRIMP zircon ages constraining the depositional chronology of the Hamersley Group, Western Australia. Aust. J. Earth Sci. 51, 621–644.

Trendall, A.F., Nelson, D.R., De Laeter, J.R., Hassler, S.W., 1998. Precise zircon U–Pb ages from the Marra Mamba Iron Formation and Wittenoom Formation, Hamersley Group, Western Australia. Aust. J. Earth Sci. 45, 137–142.

van Zuilen, M.A., Lepland, A., Arrhenius, G., 2002. Reassessing the evidence for the earliest traces of life. Nature 418, 627–630.

Vargas, M., Kashefi, K., Blunt-Harris, E.L., Lovley, D.R., 1998. Microbiological evidence for Fe(III) reduction on early Earth. Nature 395, 65–67.

Veizer, J., Clayton, R.N., Hinton, R.W., von Brunn, V., Mason, T.R., Buck, S.G., Hoefs, J., 1990. Geochemistry of Precambrian carbonates: 3-shelf seas and non-marine environments of the Archean. Geochim. Cosmochim. Acta 54, 2717–2729.

Wakeham, S.G., Amann, R., Freeman, K.H., Hopmans, E.C., Jørgensen, B.B., Putnam, I.F., Schouten, S., Sinninghe Damsté, J.S., Talbot, H.M., Woebken, D., 2007. Microbial ecology of the stratified water column of the Black Sea as revealed by a comprehensive biomarker study. Org. Geochem. 38, 2070–2097.

Waldbauer, J.R., Sherman, L.S., Sumner, D.Y., Summons, R.E., 2009. Late Archean molecular fossils from the Transvaal Supergroup record the antiquity of microbial diversity and aerobiosis. Precambrian Res. 169, 28–47.

Welch, S.A., Beard, B.L., Johnson, C.M., Braterman, P.S., 2003. Kinetic and equilibrium Fe isotope fractionation between aqueous Fe(II) and Fe(III). Geochim. Cosmochim. Acta 67, 4231–4250.

Whitehouse, M.J., Fedo, C.M., 2007. Microscale heterogeneity of Fe isotopes in >3.71 Ga banded iron formation from the Isua Greenstone Belt, Southwest Greenland. Geology 35, 719–722.

Widdel, F., Schnell, S., Heising, S., Ehrenreich, A., Assmus, B., Schink, B., 1993. Ferrous iron oxidation by anoxygenic phototrophic bacteria. Nature 362, 834–836.

Wiesli, R.A., Beard, B.L., Johnson, C.M., 2004. Experimental determination of Fe isotope fractionation between aqueous Fe(II), siderite and "green rust" in abiotic systems. Chem. Geol. 211, 343–362.

Williams, I.R., 1989. 1:100,000 series explanatory notes. In: Balfour Downs, W.A. (Ed.), Geological Survey of Western Australia. 39 pp.

Wingate, M.T.D., 1999. Ion microprobe baddeleyite and zircon ages for late Archaean mafic dykes of the Pilbara Craton, Western Australia. Aust. J. Earth Sci. 46, 493–500.

Woese, C.R., Fox, G.E., 1977. Phylogenetic structure of the prokaryotic domain: the primary kingdoms. Proc. Natl. Acad. Sci. U. S. A. 74, 5088–5090.

Xiong, J., Fischer, W.M., Inoue, K., Nakahara, M., Bauer, C.E., 2000. Molecular evidence for the early evolution of photosynthesis. Science 289, 1724–1730.

Yamaguchi, K.E., 2002. Geochemistry of Archean-Paleoproterozoic black shales: the early evolution of the atmosphere, oceans, and biosphere. Ph.D. thesis, Pennsylvania State University. 485 pp.

Yamaguchi, K.E., Johnson, C.M., Beard, B.L., Ohmoto, H., 2005. Biogeochemical cycling of iron in the Archean–Paleoproterozoic Earth: constraints from iron isotope variations in sedimentary rocks from the Kaapvaal and Pilbara Cratons. Chem. Geol. 218, 135–169.

Yamaguchi, K.E., Johnson, C.M., Beard, B.L., Ohmoto, H., 2004. Iron–sulfur–carbon contents and isotope systematics of 2.7 Ga shallow and deep facies black shales from the Hamersley Basin, Australia. Geochim. Cosmochim. Acta 68 (11 Suppl), 795.

Zerkle, A.L., House, C.H., Brantley, S.L., 2005. Biogeochemical signatures through time as inferred from whole microbial genomes. Am. J. Sci. 305, 467–502.